J Mater Sci (2010) 45:1760–1768
DOI 10.1007/s10853-009-4153-9

Effect of textural characteristics of supported metallocenes on ethylene polymerization

Fernando Silveira · Rodrigo Brambilla · Nadya Pesce da Silveira · Maria do Carmo Martins Alves · Fernanda C. Stedile · Sibele B. C. Pergher · João Henrique Zimnoch dos Santos

Received: 5 December 2009 / Accepted: 18 December 2009 / Published online: 6 January 2010

Abstract Catalyst particle size is an important parameter in the polymer industry. A series of supports with different textural properties (silicas prepared by different routes), surface sites (alumino-silicate, silica-zirconia, magnesia-silica supports, and methylaluminoxane-modified silica) and crystallinity (amorphous, lamellar, and crystalline materials) were investigated in the sequential grafting reaction of two metallocene catalysts, Cp_2ZrCl_2 and $(n\text{-BuCp})_2ZrCl_2$, in a 1:3 ratio. The catalyst systems were analyzed by Rutherford backscattering spectrometry, atomic force microscopy, small angle X-ray scattering, extended X-ray absorption fine structure spectroscopy, and nitrogen adsorption. All of the systems were shown to actively polymerize ethylene when methylaluminoxane was used as the cocatalyst. Experimental results are discussed in terms of the relationships between the radius of gyration of secondary particles and catalyst activity. A radius of gyration in the range of 8–9 nm was shown to be associated with higher catalyst activity.

F. Silveira
Braskem S.A., III Pólo Petroquímico, Via Oeste, Lote 05, Triunfo 95853-000, Brazil

R. Brambilla · N. P. da Silveira · M. do Carmo Martins Alves · F. C. Stedile · J. H. Z. dos Santos (✉)
Instituto de Química, UFRGS, Av. Bento Gonçalves, 9500, Porto Alegre 91509-900, Brazil
e-mail: jhzds@iq.ufrgs.br

S. B. C. Pergher
Departamento de Química, Universidade Regional Integrada do Alto Uruguai e das Missões (URI), Campus Erechim, CP 743, Erechim 99700-000, Brazil

Introduction

Numerous industries depend on the size of particles to improve performance or to meet specifications. For instance, particle size is a variable of significant interest to coating manufacturers, as it directly impacts the optical properties, such as the opacity, tinting strength, undertone, film appearance, and weather resistance, of the finished product. In the polymer industry, the size and shape of catalyst particles affect the catalyst performance as well as the quality of the final polymer product. Problems of particle overheating due high catalyst activity as well as the control of final particle morphology are relevant in the current polymer industry [1].

Most polymerization processes are highly exothermic, and reactor productivity is often constrained by heat transfer limitations and complex thermodynamic constraints. Dynamic changes in catalyst activity (i.e., activation and deactivation) also affect the safe regions of operation. Clearly, catalyst textural properties affect the diffusion of the cocatalyst and comonomer. Furthermore, the support structure may affect catalyst fragmentation, which thereby exposes new catalyst sites during polymerization and subsequently increases catalyst activity.

Many techniques can be used to provide information about particle size, such as ultrasonic attenuation (range of 0.1–1000 μm), electro-acoustics (0.1–10 μm), X-ray sedimentation (0.1–1000 μm), laser light diffraction (0.05–1000 μm), dynamic light scattering (0.05–1000 μm), atomic force microscopy (AFM, nm range), and scanning electron microscopy (SEM, μm range) [1].

In terms of catalyst characterization, small angle X-ray scattering (SAXS) is a powerful tool for examining the textural properties of catalyst surfaces and often provides complementary data to N_2 adsorption (BET method)

analysis. For instance, the textural properties of Raney Ni catalysts [2], the submicrostructure evolution of precipitated hydrous zirconia [3], and the aggregation and diffusion of elements in supported Pt–Au catalysts [4] have all been investigated by SAXS. Anomalous small angle X-ray scattering (ASAXS), in which data are obtained at different X-ray energies close to a metal adsorption edge, where the metal scattering strength changes and thereby provides element specificity, has been employed to study the size and composition distribution of alloy nanoparticle electrocatalysts [5].

Atomic force microscopy has been used for the determination of particle size and the degree of surface roughness of silicas [6]. This technique has long been used for the characterization of supported catalysts such as fluid-cracking catalysts (FCC) [7] or Pd/Al_2O_3 [8]. More recently, AFM has been used in the characterization of Ziegler–Natta polymerization catalysts [9].

Metallocenes represent a class of polymerization catalysts that are very active in the polymerization of olefins and can produce new commodities, especially by copolymerization reactions. It has been estimated that the polyolefin market will grow by 64% in the next decade, i.e., 3–5% per year. It is believed that the amount of polyethylene produced by metallocene catalysts will increase by 470%. Presently, the market for polyethylenes produced by metallocenes represents ca. 5–6% of the polyolefin market, which corresponds to 3–4 million tons of polymers per year [10].

For technical reasons, metallocenes must be heterogenized for industrial application. Silica is the most widely studied support in both the academic and industrial literature. Nevertheless, other types of supports have also been evaluated for the immobilization of metallocenes, with the aim of increasing catalyst activity or generating different polymer properties [11]. The microstructure of the support is very important because it can offer benefits regarding the ease of fragmentation during polymerization, which can lead to increased activity and reduced induction times.

In previous work, we reported the effect of grafting Cp_2ZrCl_2 and $(n\text{BuCp})_2ZrCl_2$ on the same support (silica), at different order and molecular ratios, on the catalyst activity and on the polymer properties. The best catalyst system was that resulting from grafting Cp_2ZrCl_2 followed by $(n\text{BuCp})_2ZrCl_2$ in a 1:3 ratio [12]. In subsequent papers, we investigated the effect of textural properties of silicas produced by different techniques (aerogel, xerogel, precipitated silicas, etc.) [13], including the effects of the chemical composition of the support surface (alumino-silicates, silica-zirconia, and magnesia-silica supports) and the effects of crystallinity (amorphous, lamellar, and crystalline materials) [14], on catalyst performance. In this paper, we focus on the particle size of the secondary particles of the support. Therefore, SAXS was employed to extract information about the radius of gyration (R_g) and fractal dimension. Complementary analyses were carried out by extended X-ray absorption fine structure (EXAFS) spectroscopy and AFM. The results regarding the Zr–C interatomic distance in the supported metallocene are discussed, as well as their catalyst activity in the polymerization of ethylene.

Experimental

Materials

All chemicals were manipulated under an inert atmosphere using Schlenk techniques. Commercial silicas (Grace 560 and Grace 480) were provided by Grace Chemical. Chrysotile was kindly provided by SAMA (Goiás, Brazil). SBA-15 was prepared at the Instituto de Tecnología Química de Valencia—ITQ-UPV (Spain). MAO-modified silica (SMAO) with 23 wt% Al/SiO_2 (Witco) and alumina (INLAB, Brazil) were used without further purification. MCM-41, MCM-22, and ITQ-22 were prepared according to published procedures [15–17]. Silica xerogel and silica-zirconia were prepared by hydrolytic and non-hydrolytic sol–gel processes, respectively [12]. Silica aerogel was synthesized at CENERG (France). Leached chrysotile was obtained according to a published procedure [18]. Furthermore, $(n\text{-BuCp})_2ZrCl_2$ (Aldrich), Cp_2ZrCl_2 (Aldrich), and MAO (Witco, 10.0 wt% toluene solution) were used as received. Toluene was deoxygenated and dried by standard techniques before use. Ethylene and argon (White Martins) were passed through molecular sieves (13 Å) prior to use. Toluene was purified by refluxing over sodium and distilled under nitrogen immediately prior to use.

Synthesis of the supported hybrid catalysts

All of the supports were activated under vacuum ($P < 10^{-5}$ bar) for 16 h at 450 °C. In a typical experiment, a toluene solution of Cp_2ZrCl_2, corresponding to 0.25 wt% Zr/SiO_2, was added to ca. 1.0 g of the pre-activated support and stirred for 30 min at room temperature. The solvent was then removed under vacuum through a fritted disk. A toluene solution of $(n\text{-BuCp})_2ZrCl_2$, corresponding to 0.75 wt% Zr/SiO_2, was added, and the resulting slurry was stirred for at least 30 min at room temperature. The resulting slurry was filtered through a fritted disk, and the solids were washed with toluene (10×2.0 cm^3) and dried under vacuum for 4 h.

The same procedure was carried out on all of the activated supports, such as MCM-22, ITQ-2, SBA-15, alumina, and silica-zirconia produced by the nonhydrolytic

sol–gel route, as well as on natural chrysotile (magnesia-silica). The resulting supported catalyst systems were designated M22, IT2, S15, ALU, NHI, and nCR, respectively, after catalyst grafting. For the silicas, the label corresponds to the commercial source: G56 for silica Grace 560, SMAO for MAO-modified silica; or to the synthetic route: AER for aerogel, HID for xerogel produced by the hydrolytic sol–gel route.

Characterization of supported catalysts

Small angle X-ray scattering

The SAXS experiments were carried out using synchrotron radiation at LNLS (Campinas, Brazil) with a wavelength $\lambda = 1.488$ nm. The beam was monochromatized by a silicon monochromator and collimated by a set of slits defining a pin-hole geometry. A CCD detector (MAR 160) located at 1449.5 mm of the sample was used to collect two-dimensional (2D) images with 2048 × 2048 pixels. The data were corrected for sample transmission and background scattering using an empty cell as a reference. Samples were placed in stainless steel sample holders closed by two mica windows. The 2D SAXS images were transformed to SAXS spectra using the FIT-2D software.

Rutherford backscattering spectrometry

Zirconium loadings in the catalysts were determined by Rutherford backscattering spectrometry (RBS) using He^+ beams with 2.0 MeV of energy incident on homogeneous compressed (12 MPa) tablets of the catalyst material. The method is based on the determination of the number and the energy of the detected particles that are elastically scattered by the Coulombic field of the atomic nuclei in the target. In this study, the Zr/Si or Zr/Al atomic ratios were determined by the heights of the signals corresponding to each of the elements in the spectra and converted to a wt% Zr/SiO_2 or Al_2O_3. For an introduction to this method and applications of this technique, the reader is referred elsewhere [19].

Nitrogen adsorption–desorption isotherms

Samples were degassed (10^{-2} mbar) at 120 °C (silica) or at 85 °C (supported catalysts) for 8 h. Adsorption–desorption nitrogen isotherms were measured at −196 °C using a Gemini 2375 (Micromeritics) instrument. Specific surface areas (S_{BET}) were determined by the Brunauer–Emmett–Teller equation ($P/P_0 = 0.05$–0.35). The mesopore size and distribution were calculated by the Barrett–Joyner–Halenda (BJH) method using the Halsey standards. Desorption branches were used.

Atomic force microscopy

Images of the supported catalyst surfaces were obtained using a Nanoscope IIIa® atomic force microscope, manufactured by Digital Instruments Co., using the contact mode technique with silicon nitride probes. The WS M 4.0 software from Nanotec Electronic S.L. was used to process the images. The samples were compressed into the form of tablets and fragments of roughly 16 mm^2 for the analysis.

Extended X-ray absorption fine structure

The EXAFS measurements were performed near the Zr K edge ($E = 17{,}998$ eV) using the Si(220) channel-cut monochromator at the XAFS 1 beamline (LNLS, Campinas, Brazil). The spectra were collected in fluorescence mode using one ionization chamber filled with argon and a Si(Li) detector. To perform the EXAFS experiments, the supported metallocene powder was compacted into a pellet and covered with Kapton® tape. All of the manipulations were performed in a dry box to avoid any oxidation reactions. The EXAFS spectra were acquired from 17,900 to 18, 900 eV in 3 eV intervals. Several scans were averaged to improve the signal-to-noise ratio.

The IFEFFIT analysis package [20] and the Winxas program [21] were used to analyze the EXAFS data. The EXAFS signals between 1.0 and 10.0 $Å^{-1}$ were Fourier transformed with a k^1 weighting and a Bessel window. Structural parameters were obtained from least-squares fitting in k and R space using theoretical phase shift and amplitude functions deduced from the FEFF7 code [20]. The input for the FEFF7 code was provided by the ATOMS program. In the fitting procedure, the amplitude reduction factor (S_0^2) was close to 1.0 for all samples, and the threshold energies (E_0) for the Zr–C and Zr–O pairs were −7.5 and −3.5 eV, respectively.

Polymerization reactions

Polymerizations were performed in toluene (0.15 L) in a 0.30-L Pyrex glass reactor connected to a constant temperature circulator equipped with mechanical stirring and inlet ports for argon and monomers. For each experiment, the catalyst system (a mass corresponding to 10^{-5} mol L^{-1} of Zr) was suspended in toluene (0.01 L) and transferred into the reactor under argon. The polymerizations were performed under an atmospheric pressure of ethylene at 60 °C for 30 min at Al/Zr = 1000, using MAO as the cocatalyst. Acidified ethanol (HCl) was used to quench the reactions. The reaction products were separated by filtration, washed with distilled water, and finally dried under reduced pressure at 60 °C.

Polyethylene characterization

Gel permeation chromatography

The molar masses and molar mass distributions were determined with a Waters CV plus 150 °C high-temperature gel permeation chromatography (GPC) instrument, equipped with a viscosimetric detector, and three Styragel HT-type columns (HT3, HT4, and HT6) with an exclusion limit of 1×10^7 for polystyrene. 1,2,4-trichlorobenzene was used as the solvent with a flow rate of 1 cm^3 min^{-1}, and the analyses were performed at 140 °C. The columns were calibrated with polystyrenes that had standard narrow molar mass distributions and with linear low-density polyethylenes and polypropylenes.

Scanning electron microscopy

SEM experiments were carried out on a JEOL JSM/6060 electron microscope. The polymers were initially fixed on carbon tape and then coated with gold by conventional sputtering techniques. The employed accelerating voltage was 10 kV for SEM.

Results and discussion

The supports and supported catalysts were analyzed by SAXS. Taking into account the q intermediate region in the SAXS curve, the coefficient values (slopes) were calculated for the different systems. This coefficient is related to the fractal geometry of the silica particles, as shown in Scheme 1.

According to Scheme 1, for α values between 1 and 3, the support particle presents a structure described as mass fractal. If the α value is between 3 and 4, the support particles are formed by a surface fractal, while for $\alpha = 4$, the silicas are constituted of dense and uniform particles related to typical Porod structures.

The SAXS profiles also allowed us to evaluate the radius of gyration (R_g) of the particles from the Guinier regime that obey the condition $qR_g \ll 1$, i.e., $q \to 0$; the intensity (I) could be approximated by the Gaussian function given by Eq. 1.

$$I(q) = I_0 e^{\frac{-q^2 R_g^2}{3}} \quad (1)$$

The radius of gyration (R_g) could be assessed by fitting the experimental data using a linearized version of Eq. 1 and algebraic manipulations.

Figure 1 shows SAXS curves, plotted as Log I × Log q, for the different silica supports.

According to Fig. 1, the slopes were dependent on the nature of the silica used. The SAXS curve of commercial silica G56 presented a slope of −2.8, which can be attributed to particles with a mass fractal structure [22]. The mass fractal structures are open, like low-density polymeric structures (fern-like). These structures evidence growth by cluster–cluster aggregation (CCA). In CCA, monomers are depleted at an early stage of the growth process, so further growth must occur exclusively between clusters. Strong mutual screening of cluster interiors leads to ramified objects characterized by a mass fractal dimension. On the other hand, the SAXS curve of commercial silica G48 showed a slope of −3.1, which characterizes a surface fractal structure [22]. Surface fractal structures are composed of dense nuclei with rough surfaces. These surface fractal structures evidence growth by monomer–cluster aggregation (MCA).

In general, silicas are produced in the industry from sodium silicate solutions. Therefore, this observed difference in the fractal structure could be attributed to the synthesis conditions, such as the pH, silicate concentration, and drying conditions. For silica synthesized from tetraethoxysilane (TEOS) by a hydrolytic sol–gel route under acidic conditions (HYD), the SAXS curve presented a slope of −2.4, which can be attributed to particles with a mass fractal structure, evidence of growth by CCA as in the case of commercial silica G56. The mass fractal structure can also be observed for the leached chrysotile support.

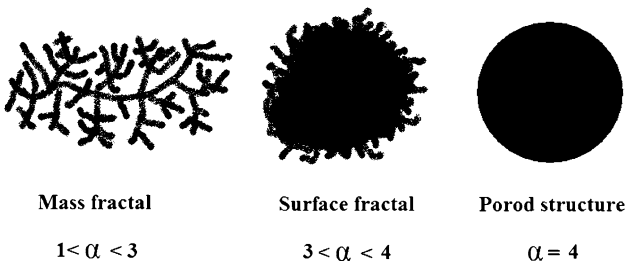

Scheme 1 Possible fractal geometries of silica particles

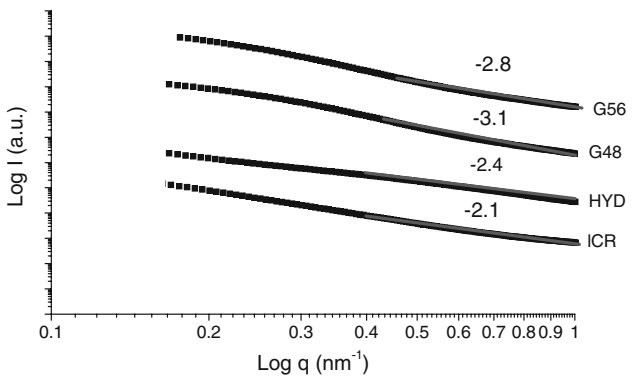

Fig. 1 SAXS curves, plotted as Log I × Log q, for the different silica supports

There were no differences among the SAXS profiles of the supports and those of the silica-supported catalysts. The SAXS curves of aerogel silica (AER) (not shown) presented a power-law regime with $\alpha = 2.2$, characteristic of a mass fractal structure [22].

Another set of supports including mesoporous materials bearing sites differing in their chemical nature (alumino-silicates, silica-zirconia, magnesia-silica support, and MAO-modified silica) was also analyzed by SAXS. Figure 2 shows the typical scattering profiles of alumino-silicates (S15 and IT2).

The SAXS curve of S15 (Fig. 2a) presented a long-range ordering that is evidenced by three diffraction peaks at $q = 0.33$, 0.57, and 0.66 with corresponding d-spacings of 19.1, 11.0, and 9.5 nm. The unit cell parameter a, which was calculated from the (10) diffraction peak according to the equation $a = 2 \times \mathrm{d10}/\sqrt{3}$, is 22.1 nm [23]. For IT2, the SAXS curve (Fig. 2b) showed a low long-range ordering, evidenced by three low-intensity diffraction peaks at $q = 0.81$, 1.40, and 1.62 with corresponding d-spacings of 7.8, 4.5, and 3.9 nm. The unit cell parameter a, which was calculated from the (10) diffraction peak according to the equation $a = 2 \times \mathrm{d10}/\sqrt{3}$, is 9.0 nm [23].

The SAXS curves of M22 and M41 (not shown) did not present diffraction peaks, which means that these samples do not have long-range ordering. However, the SAXS curves showed a power-law regime with α equal to 2.5 and 2.7, respectively, characteristic of a mass fractal structure [22].

Figure 3 shows SAXS curves, plotted as Log $I \times$ Log q, for the different metal modified silica supports.

According to Fig. 3, the linear fit of the SAXS curves for the metal modified silicas results in different slopes. Therefore, these systems present different fractal structures. The silica-zirconia synthesized by a nonhydrolytic sol–gel route presented a slope of −3.8, which can be attributed to a surface fractal. For commercial silica modified with methylaluminoxane (SMAO), a slope of −2.4, characteristic of a mass fractal structure, can be observed. In the case of silica-magnesia nCr (natural chrysotile), a slope of −3.3, which characterizes a surface fractal structure, is observed [22].

The supported catalysts were further analyzed by AFM. Figure 4 shows some micrographs of the silica-supported catalysts.

According to Fig. 4, the particles in the nanometer range are agglomerates formed by particle aggregation with sizes of ca. 80 nm for G56 and 40 nm for HID.

Figure 5 illustrates some micrographs of the employed resulting supported catalysts in the case of alumino-silicates, silica-zirconia, and magnesia-silica supports.

For the catalyst IT2, the aggregates were in the range of 57–61 nm. In the case of M22, the aggregates observed by AFM measured roughly 75 nm. For S15, the AFM images revealed particles in the range of 93–125 nm. For SMAO, the observed aggregates measured ca. 90 nm. In the case of nCR, fibers of 47 and 67 nm in width were observed. In

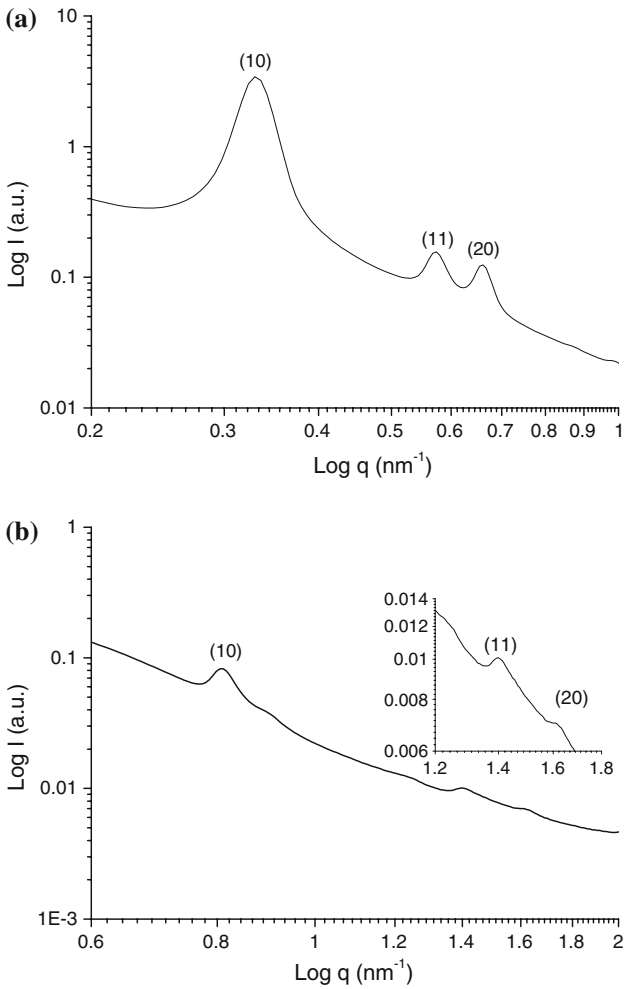

Fig. 2 SAXS curves, plotted as Log $I \times$ Log q, for the different alumino-silicates **a** S15 and **b** IT2

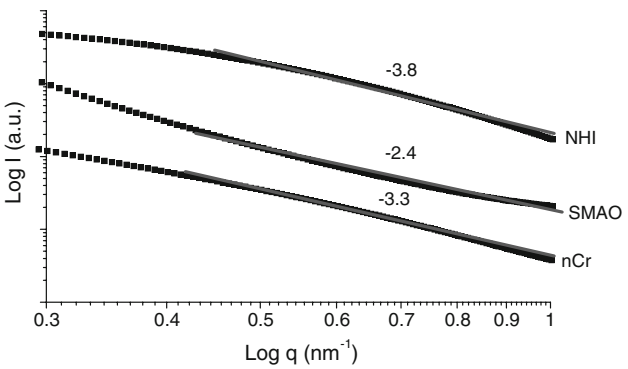

Fig. 3 SAXS curves, plotted as Log $I \times$ Log q, for the different metal modified silicas

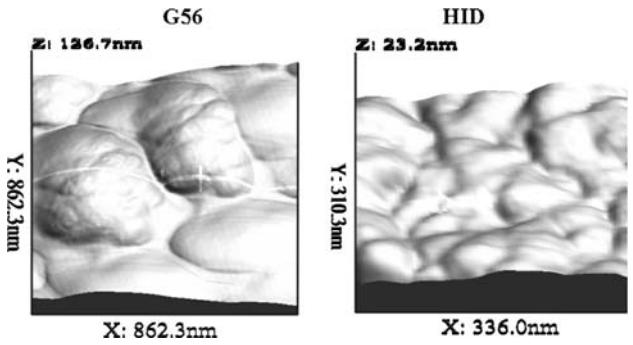

Fig. 4 AFM images of two supported catalysts, G56 and HID

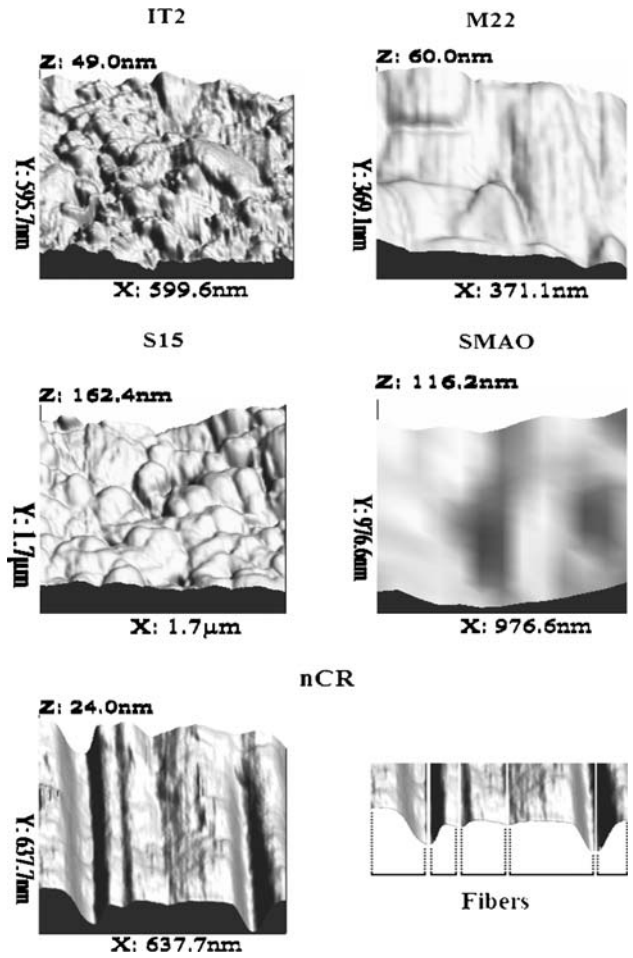

Fig. 5 AFM images of IT2, M22, S25, SMAO, and nCR

some fibers, plates of 50 nm were observed. A similar behavior was observed in the images obtained by AFM in the micron range. Chrysotile is a natural nanostructured material with fibers, in which the thickness was reduced from 0.2 to 0.17 μm, as shown in Fig. 6.

Table 1 presents data reporting grafted metal content, textural properties, and catalyst activity in ethylene polymerization.

According to Table 1, the grafted metal content varied from 0.15 to 1.00 wt% Zr/SiO_2 or wt% Zr/Al_2O_3, depending on the support, but the textural characteristics of the materials were distinct. No clear trend was observed between particle size, grafted metal content, surface area, pore diameter, fractal structure, radius of gyration of the catalysts, the catalyst activity, or the molar mass of the polymers. Therefore, to better investigate the effect of catalyst properties on catalytic activity and on the molar mass of the polymers, the set of data was analyzed by cluster analysis. The results of this analysis are shown in Fig. 7.

According to Fig. 7, the different systems can be divided into three clusters containing systems that present similar textural properties and catalytic performance. The first group is formed by commercial silicas: G56, G55, G48, and SMAO. The systems of this cluster presented a high catalyst activity, which can be attributed to a combination of large pores, relatively large surface areas, and particle sizes of roughly 50 μm. The large pores and surface areas of these systems should reduce the diffusion problem to the monomer or cocatalyst level, improving the catalyst activity. The particle size is related to the fragmentation of the catalyst system. In general, larger particles fragment more easily, resulting in higher catalyst activity. From both a technological and a macroscopic point of view, particles as large as 50 μm are ideal for most polyolefin polymerization processes. For SMAO, the high catalyst activity can also be attributed to the mobility of metallocene immobilized on MAO moieties on the silica surface. The second group is constituted by some metal-modified silicas (NHI and nCr) and alumina (ALU). The systems of this cluster presented a low catalyst activity, which can be partially attributed to the relatively low-specific surface area of the supported catalysts (14–103 $m^2\ g^{-1}$). This low surface area should reduce the monomer or cocatalyst access to the active centers, decreasing the catalyst activity. For nCr and ALU, this low catalyst activity can also be attributed to the small grain size of the supported catalysts (0.2 and 0.4, respectively). The last group contains the catalytic systems that presented moderate-to-high catalyst activity. This included silica-based materials (HID and lCr) and other supports with high-specific surface areas, such as AER and mesoporous ordered materials (S15, IT2, M22, and M41). In this group, the high-specific surface area justifies the high catalyst activity in relation to the second group. However, the lower activity in comparison to that observed for the first group can be attributed to the smaller pore and particle size, which prevents monomer or cocatalyst access to the active sites. Additionally, the small grain size inhibits the supported catalyst fragmentation, leading to a decrease in catalyst activity.

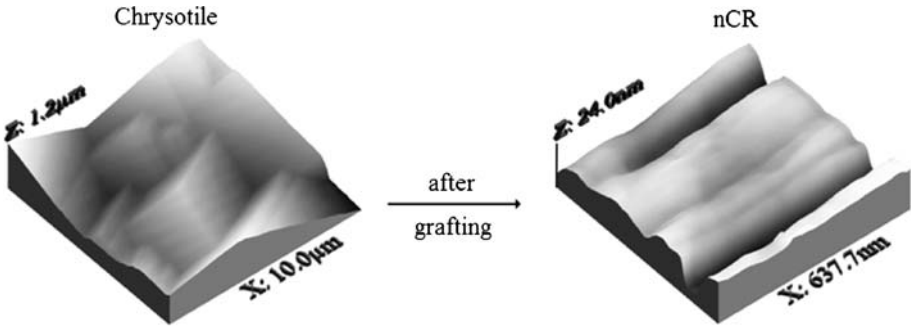

Fig. 6 AFM image of nCR **a** after and **b** before zirconocene grafting

Table 1 Grafted metal content, textural characteristics, catalyst activity and polymer characteristics of the investigated supported metallocenes

Supported catalyst	Grafted metal content (wt% Zr/SiO_2 or Al_2O_3)	Surface area ($m^2\ g^{-1}$)	Pore diameter (Å)	Particle diameter (μm)	Catalyst activity (kg PE mol $Zr^{-1}\ h^{-1}$)	Mw (kg mol^{-1})	α	R_g (nm)
G56	0.51	200	145	49	4280	423	2.8	8.5
G55	0.33	244	128	50	2220	338	2.9	8.8
G48	0.35	249	118	51	5310	258	3.1	8.3
HYD	0.50	341	39	77	1680	356	2.4	3.9
AER	0.15	462	58	0.4/1.6	3537	343	2.2	2.8
M41	0.84	768	24	0.2	880	484	2.7	–
lCR	0.20	226	39	0.1	1927	378	2.1	7.6
NHI	0.41	18	36	83	720	306	3.8	5.7
ALU	0.90	103	42	0.4	853	351	4.0	5.3
SMAO	1.00	99	84	49	6560	388	2.4	8.1
S15	0.42	463	50	0.2	3200	273	–	–
IT2	0.61	478	14	0.1	1260	477	–	–
M22	0.51	313	19	0.1	1467	275	2.5	–
nCR	0.21	14	39	0.2	400	254	3.3	6.1

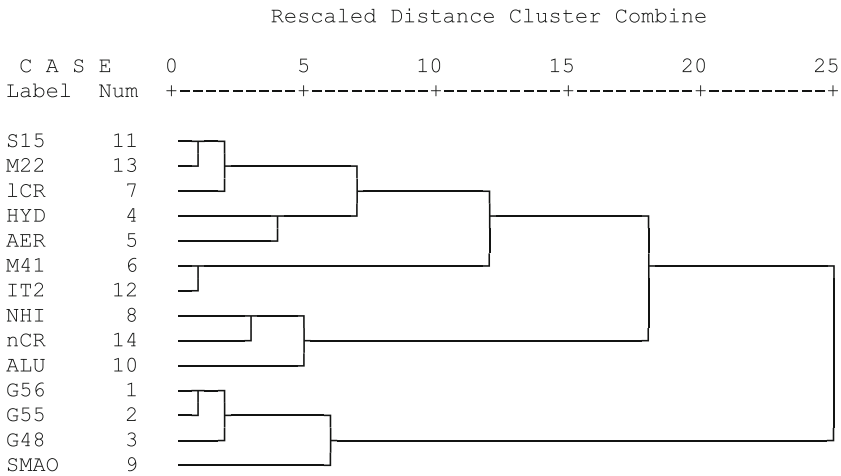

Fig. 7 Dendrogram obtained by the Ward method in cluster analysis

Although the effect of grain size of supported metallocenes on the activity of ethylene polymerization has been reported, the effect of R_g of secondary particles in these systems to our knowledge has been not investigated in the literature. Therefore, the R_g data measured by SAXS were correlated with the catalyst activity of ethylene polymerization, as shown in Fig. 8.

According to Fig. 8, the radius of gyration (R_g) of secondary particles of the supported catalyst influenced the catalyst activity of ethylene polymerization. Comparing the

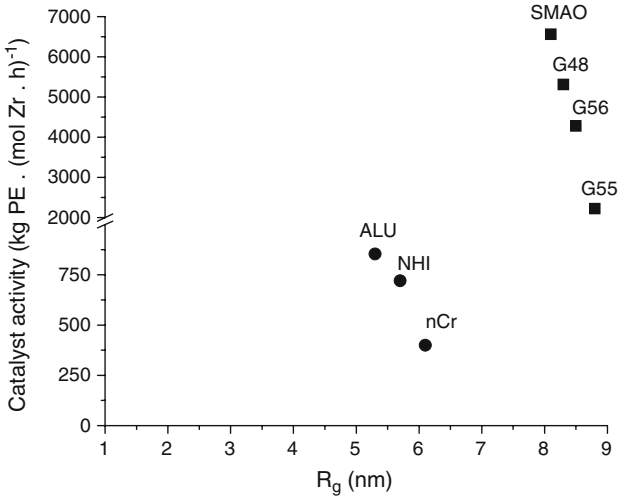

Fig. 8 Influence of R_g of secondary particles in the supported catalyst on catalyst activity of ethylene polymerization for the (*filled square*) Commercial silicas and (*filled circle*) alumina/metal-modified silica clusters

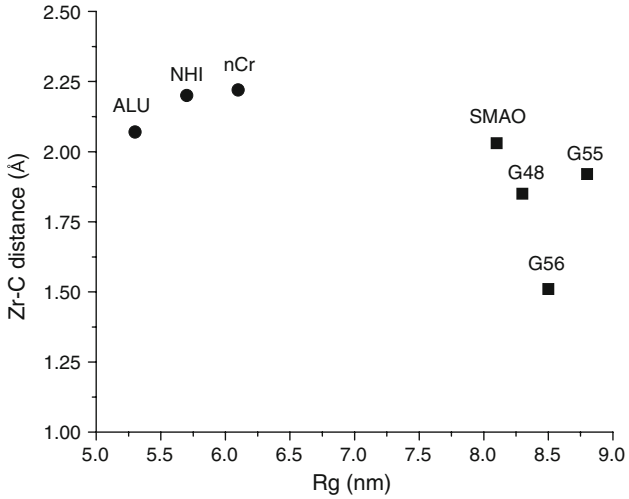

Fig. 9 Influence of R_g of secondary particles in the supported catalyst on the Zr–C distance of the metallocene complex for the (*filled square*) commercial silicas and (*filled circle*) alumina/metal-modified silica clusters

results obtained for these two groups, it can be observed that R_g in the range of 8–9 nm favors catalyst activity. However, for the same group, a decrease in R_g of secondary particles results in increased catalyst activity of ethylene polymerization. For the group of mesoporous ordered materials, there was no correlation between catalyst activity and the radius of gyration (R_g).

No clear trend could be observed between the particle pore size and Mw. However, for commercial silicas G48, G55, and G56, the increase in pore size resulted in an increased Mw.

In a previous work, we observed that the pore diameter of the support can affect the structure of the grafted metallocene structure, as evaluated by the Zr–C interatomic distance determined by EXAFS [13]. In this study, we investigated the effect of R_g of secondary particles on the structural characteristics of the supported metallocenes. Figure 9 shows a correlation between the Zr–C distance of the metallocene complex and the R_g of secondary particles for the supported metallocenes. It is worth noting that these values represent mean interatomic values of the supported species.

According to Fig. 9, for the first group of catalyst systems, as R_g increases, there is a reduction in the Zr–C interatomic distance. The G55 supported catalyst does not follow this trend, probably due to other textural parameters, such as pore fraction and mean pore size distribution, which should be influencing the structure of grafted metallocene. For G48, G56, and SMAO, the pore fraction was in the range of 1.5–1.9%, while in the case of G55, a pore fraction of 6.4% was determined. Besides a broader mean pore size distribution was observed for this system [13]. For the second group of systems, the inverse trend is observed. As R_g increases, there is an increase in the Zr–C interatomic distance. These results suggest that the size of secondary particles of the support influences the structure of the supported metallocene complex. However, the observed trend was dependent on other textural characteristics of the supported metallocene systems. For the group of mesoporous ordered materials, there was no correlation between the Z–C interatomic distance and the radius of gyration (R_g).

The morphology of the resulting polyethylene was investigated by SEM. Figure 10 shows SEM micrographs for polymers prepared with the G48, NHI, and S15 systems.

According to Fig. 10, the polyethylenes obtained by using supports with different textural characteristics showed distinct morphologies. The polymer obtained with the G48 system showed no particular morphology. For NHY and S15, a fiber-like morphology can be observed, suggesting a polymerization by extrusion mechanism, in which the polymer chain growth takes place within the mesopores up to the particle surface [24]. In addition, the fiber morphology of the polymer obtained with the S15 system is aligned, which demonstrates the influence of pore organization, as shown by SAXS data, on fiber orientation.

Conclusion

The grafting of metallocenes on the surface of different supports preserves the radius of gyration and the fractal geometry of bare supports. However, the radius of gyration

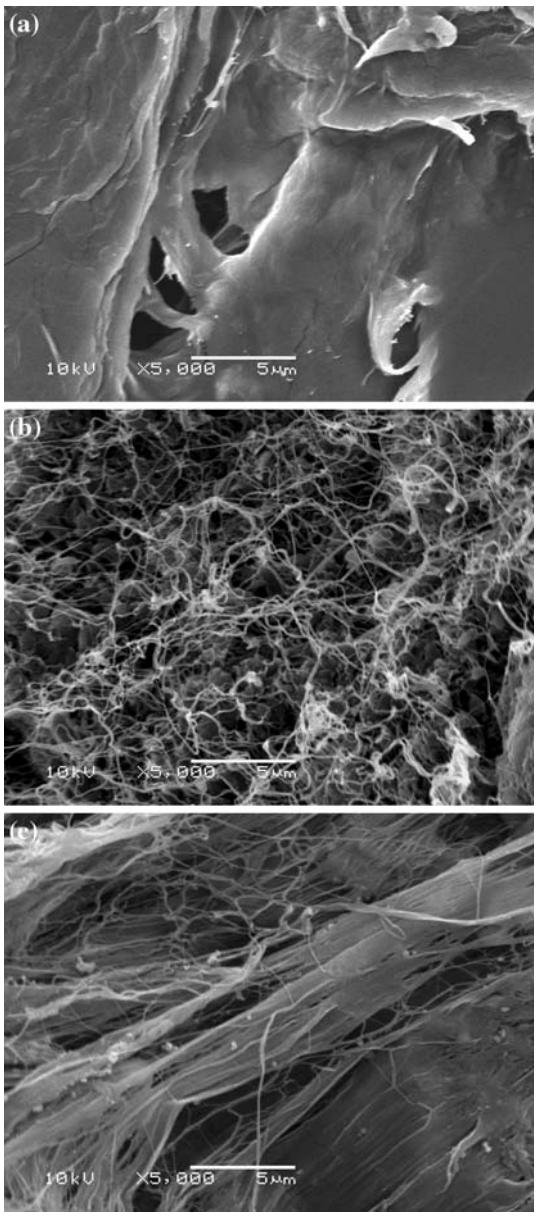

Fig. 10 SEM micrographs of polyethylene obtained with different catalyst systems: **a** G48 (commercial silica), **b** NHI (metal-modified silica), and **c** S15 (ordered mesoporous material)

of secondary particles affects the structure of the grafted metallocene, as observed in the Zr–C interatomic distances.

Cluster analysis allowed us to separate the supported catalysts into three groups of systems according to their textural properties and performance on ethylene polymerization, namely, commercial silicas, alumina and metal-modified silicas and mesoporous ordered materials. It has been shown that the use of supports with large surface area and grain size, large pores and secondary particles in the range of 8–9 nm leads to supported systems with high activity in ethylene polymerization. This result was attributed to the easier catalyst fragmentation, which in turn may provide better monomer diffusion during the polymerization process.

Acknowledgements This work was partially financed by CNPq. The authors thank LNLS for measurements on the SAXS (Project SAXSS1-5296) and EXAFS beamlines (Project D04B XAFS1#5839). Mr. William Bretas Linares from SAMA is especially thanked for providing chrysotile samples.

References

1. Merkus HG (2009) Particle size measurements: fundamentals. Practice, Quality, Springer
2. Rodella CB, Kellermann G, Francisco MSP, Jordão MH, Zanchet D (2008) Ind Eng Chem Res 47:8612
3. Yanwei Z, Yubao Z (2002) J Colloid Interface Sci 247:100
4. Bertin V, Bosch P, Del Angel G, Gomez R, Barbier J, Marecot P (1995) J Chim Phys et Phys Chim Biolog 92:120
5. Yu CF, Koh S, Leisch JE, Toney MF, Strasser P (2009) Faraday Disc 140:283
6. Paredes JI, Martínez-Alonso A, Tascón JMD (2003) Micropor Mesopor Mater 65:93
7. Occelli ML, Gould SAC (2004) Fluid catalytic cracking VI: preparation and characterization of catalysts, vol 149. Elsevier, Amsterdam, p 71
8. Lee KH, Catani R, Miglio R, Wolf EE (1997) Catal Deact 111:463
9. Andoni A, Chadwick JC, Niemantsverdriet HJW, Thüne PC (2008) J Catal 257:81
10. Chum PS, Swogger KW (2008) Prog Polym Sci 33:797
11. Severn JR, Chadwick JC, Duchateau R, Friederichs N (2005) Chem Rev 103:4073
12. Silveira F, Pires GP, Petry CF, Pozebon D, Stedile FC, Dos Santos JHZ, Rigacci A (2007) J Mol Catal A Chem 265:167
13. Silveira F, Alves MCM, Stedile FC, Pergher SB, Rigacci A, Dos Santos JHZ (2009) J Mol Catal A Chem 298:40
14. Silveira F, Petry CF, Pozebon D, Pergher SB, Detoni C, Stedile FC, Dos Santos JHZ (2007) Appl Catal A Gen 333:96
15. Kim JM, Kwak LH, Jun S, Ryoo R (1995) J Phys Chem 99:16742
16. Pergher SBC, Corma A, Fornés V (2003) Quim Nov 26:795
17. Corma A, Fornés V, Pergher SB, Maessen TLM, Buglass JG (1998) Nature 396:353
18. Fonseca MG, Oliveira AS, Airoldi C (2001) J Colloid Interface Sci 240:533
19. Stedile FC, Dos Santos JHZ (1999) Phys Stat Sol 173:123
20. Ressler T (1998) J Synch Rad 5:118
21. Rehr JJ, Albers RC (2000) Rev Mod Phys 72:621
22. Brinker CJ (2006) In: Bergna HE, Roberts WO (eds) Colloidal silica: fundamentals and applications. CRC press, Boca Raton, p 615
23. Zeleňák V, Badaničová M, Halamová D, Čejka J, Zukal A, Murafa N, Goerigk G (2008) Chem Eng J 144:336
24. Harrison D, Couter IM, Wang S, Nistala S, Kuntz BA, Pingeon M, Tian J, Collins S (1998) J Mol Catal A Chem 128:65